Macromolecules

Article

pubs.acs.org/Macromolecules

Phase Behavior of a Hydrogen-Bonded Polymer with Lamella-to-Cylinder Transition: Complex of Poly(4-vinylpyridine) and Small Dendritic Benzoic Acid Derivative

Shao-Jie Wang, Yan-Shuang Xu, Shuang Yang,* and Er-Qiang Chen*

Beijing National Laboratory for Molecular Sciences, Department of Polymer Science and Engineering and Key Laboratory of Polymer Chemistry and Physics of Ministry of Education, College of Chemistry and Molecular Engineering, Peking University, Beijing 100871, China

Supporting Information

ABSTRACT: Phase behavior of a supramolecular system based on poly(4-vinylpyridine) (P4VP) and 3,4,5-tris(dodecyloxy)benzoic acid (TDBA) [P4VP(TDBA)$_x$, where x is the molar ratio of TDBA to P4VP repeating unit] was investigated by means of FTIR, differential scanning calorimetry, polarized optical microscopy, and X-ray scattering method. The intermolecular hydrogen-bonding interaction between P4VP and TDBA is confirmed by FTIR. While almost all of the added TDBA molecules are hydrogen bonded to the P4VP chains at $x < \sim 0.60$, the hydrogen-bonding interaction becomes incomplete at $x > 0.60$ and saturates at $x > 0.90$. The phase structure of P4VP(TDBA)$_x$ is composition dependent. At $x < \sim 0.30$, the complex is homogeneous. With $\sim 0.30 < x < \sim 0.60$, P4VP(TDBA)$_x$ forms a lamella phase, of which the long period is proportional to $1/x$. Further adding TDBA causes a lamella-to-cylinder transition. At $x > \sim 0.60$, the lattice parameter of the cylinder or hexagonal columnar (Φ_H) phase decreases with increasing x. Considering the microphase separation between the polar part and the nonpolar part of alkyl tails, the lamella-to-cylinder transition can be understood using a volumetric argument. We consider that the large nonpolar part of TDBA enhances the microphase separation of P4VP(TDBA)$_x$, and moreover, the fan-like shape of TDBA facilitates the formation of Φ_H phase. We also roughly estimated the domain size of the P4VP chains in the microphase-separated mesophase. For both the lamellar and Φ_H phase, increasing x results in stronger confinement on the P4VP chains. During the lamella-to-cylinder transition the confinement imposed by the TDBA molecules may be partially released, which favors the Φ_H phase formation.

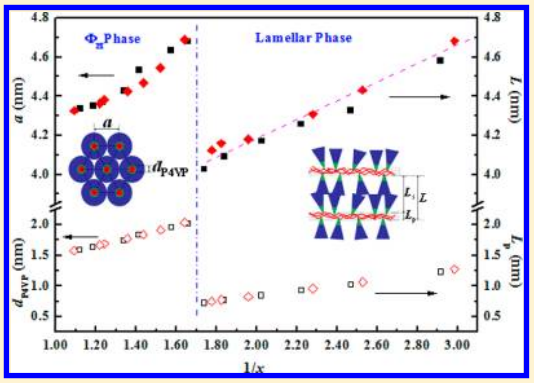

INTRODUCTION

Complexation between a appropriate linear polymer and a small ligand (e.g., surfactant) can result in a graft-copolymer-like structure, which has attracted much attention in the past years.[1−6] The noncovalent interactions includes electrostatic interaction,[7−11] hydrogen bonding,[12−15] metal−ligand coordination bond,[16,17] etc. Different from the covalent bonded graft copolymer, the polymer−ligand complex is dynamic one. The properties of the complex can be easily tuned by changing the components of polymer and small molecule, which paves a facile way for the preparation of functional materials. Thermodynamically, two key factors govern the phase behaviors of the mixture of polymer and ligand: one is the strength of polymer−ligand interaction, and the other is the segregation among the different moieties with different chemical structures.[18] The latter factor may be simply associated with polar−nonpolar repulsion, considering that the complementary binding sites of the polymer and ligand are polar ones and the ligand usually bears the nonpolar aliphatic tail. When both the specific interaction of polymer−ligand and the repulsion are strong enough, the complex system will exhibit microphase-separated ordered structures. On the other hand, if the association is too weak, the repulsion may dominant the phase behavior with the extreme case of macrophase separation.[19]

As the polyelectrolyte−surfactant system possesses the rather strong ionic bond and repulsion interaction, well-ordered mesomorphic structure is frequently observed.[20−23] However, for the complexes based on hydrogen bonding, to realize the microphase-separated structure on a nanometer scale, a balance between the intermolecular association and polar−nonpolar repulsion needs to be carefully adjusted.[18,24] For example, ten Brinke and Ikkala et al. studied the critical interaction strength for surfactant-induced mesomorphic structures in the systems based on poly(4-vinylpyridine) (P4VP).[18] They find that alkylcarboxylic acid such as dodecanoic can have sufficiently strong hydrogen-bonding interaction with P4VP, resulting in a density fluctuation which can be detected by small-angle X-ray

Received: August 27, 2012
Revised: October 15, 2012
Published: October 24, 2012

scattering. However, the tendency toward dimerization of the aliphatic acid and also the weak polar−nonpolar repulsion disfavors the formation of microphase-separated structure, and thus the P4VP−aliphatic acid mixtures are just homogeneous. On the contrary, Goh et al. demonstrate that when using poly(1-vinylimidazole) (PVI), which is a stronger base than P4VP, the PVI−aliphatic acid complex can form the well-ordered lamellar phase.[25]

So far, most of the mesophases observed in polymer−ligand complexes are lamellar or smectic. It seems to be a quite reasonable consequence when rod-like mesogenic molecules[26−30] or linear nonmesogenic molecules such as alkylphenol molecules[18,31] are used as the ligand. Of particular interest is to ask in what a situation of polymer−ligand complex a mesophase structure other than lamella can be obtained. As theoretically predicated by Fredrickson,[32] with a sufficiently high grafting density, the dynamically bonded side chains of polymer−ligand complex will interact with each other due to the excluded volume effect, and consequently, the conformation of the complex is no longer a coil one but a more extended rod. In this case, one can speculate that the parallel packing of rod-like complex with a bottle-brush structure should facilitate the formation of cylindrically microphase-separated structure, analogous to side-chain polymer with liquid crystalline columnar (Φ) phase.[33,34] Some Φ phases have been realized in polyelectrolyte−surfactant systems. Antonietti et al. report that the complex formation of poly(acrylate acid) (PAA) and dodecyltrimethylammonium chioride can result in a highly order liquid crystalline phase with PAA cylinders embedded in a continuous alkyl matrix, which is due to that the steric effects prevent the parallel orientation of the alkyl chains.[35] It is worthy to note that the polyelectrolyte−surfactant systems containing nonlinear shaped ligands can form the Φ phase more easily. Beginn et al. studied the complexation behavior of P4VP and a mesogenic wedge-shaped sulfonic acid.[36] It is found that at the degree of neutralization higher than 80% the complex forms a hexagonal columnar (Φ_H) phase. Another example is given by Tong et al.[37] They investigated the systems of poly(ethylenimine) (PEI) and poly(alkylamine hydrochloride) (PAH) complex with small dendritic amphiphiles. While the PEI-based complexes render lamellar structures, the X-ray diffraction results clearly show that the PAH−dendritic amphiphile complexes pack into Φ_H phase. According to Tong et al., the location of binding sites on the host polymer is crucial with respect to the Φ_H phase formation. Nevertheless, we can see clearly that the wedge or fan-like shape of the ligands plays an important role.

In this paper, we study the hydrogen-bonding-based complexation of P4VP and a small molecule of 3,4,5-tris(dodecyloxy)benzoic acid (TDBA) (see Scheme 1). Compared with alkylcarboxyl acid surfactants, this benzoic acid derivative should be able to interact more strongly with the pyridine group of P4VP. On the other hand, TDBA contains three dodecyl tails rather than one, which can result in more repulsion interaction and thus should lead to better microphase separation. One aim of our research is to explore the possibility of Φ_H formation in the polymer−ligand complex based on hydrogen bonding. ten Brinke and Ikkala suggest that a cylindrical structure may be obtained when the surfactant molecules bearing enough long alkyl tails are used in the hydrogen-bonding system.[24] Here, we consider that the TDBA molecule with fan-like shape should be a more straightforward candidate for the construction of Φ_H phase.

Scheme 1. Structure of P4VP and the Ligand of TDBA, Which Can Form Intermolecular Hydrogen-Bonding Interaction

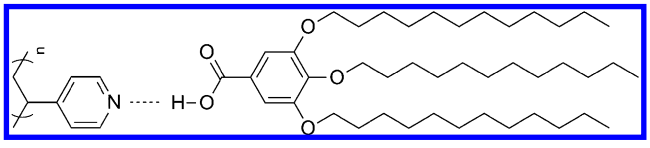

Using various techniques, we investigated the phase behavior of the complex of P4VP and TDBA with different compositions, denoted as P4VP(TDBA)$_x$ (the value of x indicates the molar ratio of TDBA to the P4VP repeating unit). The hydrogen-bonding interaction between the benzoic acid and pyridine was confirmed by Fourier transform infrared spectroscopy (FTIR). Quantitative analysis of the FTIR result shows that the fraction of hydrogen-bonded pyridines increases linearly with the addition of TDBA at $x < \sim 0.60$ and leaves off at $x > \sim 0.90$. We mainly focused on the samples with x ranged from 0 to 1 where the macrophase separation did not occur. The phase behavior of P4VP(TDBA)$_x$ can be separated into three regimes with respect to x. At $x < \sim 0.30$, the complex is homogeneous. There is a lamellar phase with the long period proportional to $1/x$ for $\sim 0.30 < x < \sim 0.60$, in agreement with that reported by ten Brinke and Ikkala.[38] Further adding TDBA leads to a lamella-to-cylinder transition. For the samples with $x > \sim 0.60$, the small-angle X-ray scattering (SAXS) result indicates the formation of Φ_H phase, of which the dimension is reduced with x. Considering the microphase separation between the polar and nonpolar parts of P4VP(TDBA)$_x$, the lamella-to-cylinder transition can be understood based on a volumetric argument. Furthermore, we deduced the variation of P4VP domain dimension in the lamellar and Φ_H phase, which might be correlated to the change of P4VP conformation from oblate coil to extended one when the phase structure is varied from lamellar to Φ_H phase.

EXPERIMENTAL SECTION

Materials. Two P4VP samples (M_n = 81 500 g/mol, PDI = 1.18; M_n = 19 000 g/mol, PDI = 1.15), denoted as P4VP$_{82K}$ and P4VP$_{19K}$, respectively, were purchased from Polymer Source Inc. They were dried in vacuum at 60 °C for 2 days prior to use. The benzoic acid molecule TDBA was synthesized according to ref 39. After careful purification, the purity of TDBA exceeded 99.9%, as tested by ^{1}H NMR, ^{13}C NMR, mass spectroscopy, and elemental analysis. All the other chemicals were obtained from Beijing Chemical Co. and were used as received.

Sample Preparation. The complexes of P4VP(TDBA)$_x$ with different molar ratio x of TDBA to the repeating unit of P4VP were prepared from chloroform solution. In each case, TDBA and chloroform were first mixed together until a clear solution was obtained. P4VP was subsequently added, followed by mechanical stirring for about 12 h at room temperature. The solution concentration was kept low (~10 mg/mL) to ensure homogeneous complex formation. Afterward, the solution was cast on the PTFE plate to evaporate chloroform. The samples were further dried at 60 °C in vacuum at least for 2 days and were thereafter stored in a desiccator.

Infrared Spectroscopy. Infrared spectra were obtained using a Bruker VECTOR22 FTIR spectrometer. Samples were prepared by casting one drop of the chloroform solution (~10 mg/mL) directly on potassium bromide crystals. The drying process of FTIR samples was same as that mentioned above. The FTIR measurements were taken at room temperature.

dx.doi.org/10.1021/ma301783h | Macromolecules 2012, 45, 8760−8769

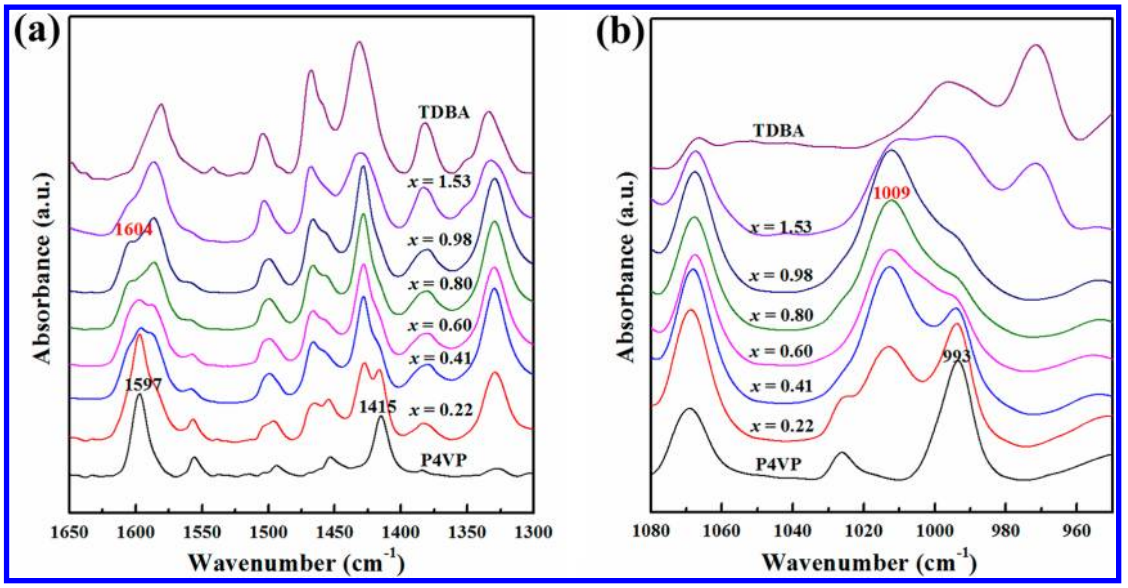

Figure 1. FTIR spectra of $P4VP_{82K}(TDBA)_x$ with various x: (a) 1300−1650 cm^{-1} region; (b) 950−1080 cm^{-1} region. For comparison, the spectra of pure $P4VP_{82K}$ and TDBA are also shown.

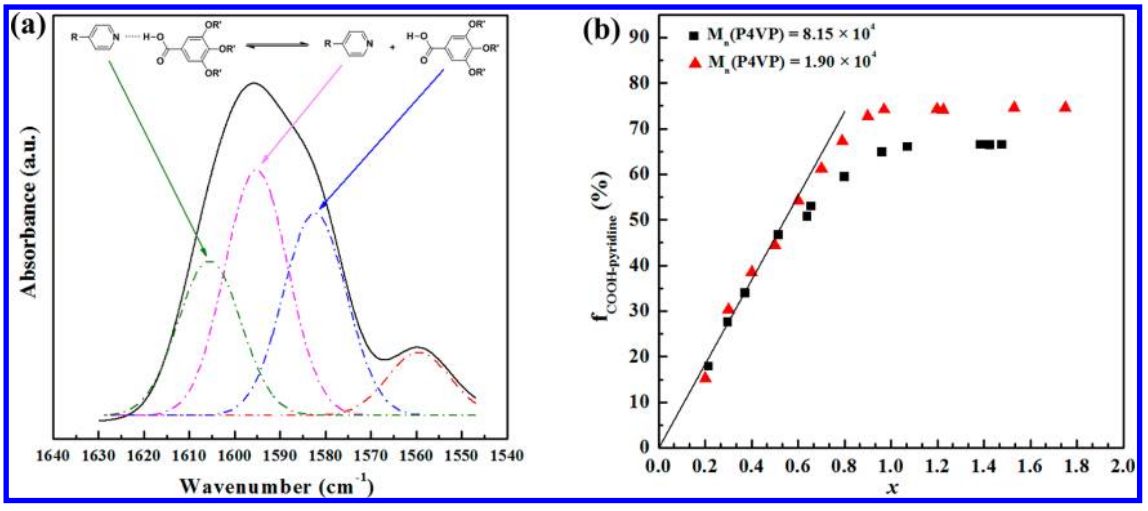

Figure 2. (a) Illustration of deconvolution of the IR absorption peak in the region of 1545−1630 cm^{-1}. (b) Fractions of hydrogen-bonded pyridines ($f_{COOH-pyridine}$) of $P4VP_{82K}(TDBA)_x$ and $P4VP_{19K}(TDBA)_x$ at a function of molar ratio x.

Differential Scanning Calorimetry (DSC). A PerkinElmer Pyris I DSC with a mechanical refrigerator was used to investigate the thermal properties of $P4VP(TDBA)_x$. The temperature and heat flow were calibrated using standard materials such as benzoic acid and indium. The dried samples were encapsulated in a sealed aluminum pan with the sample weight of ~5 mg. All the samples were first melted at 160 °C for 5 min to erase the thermal history and then cooled to −15 °C at a rate of 1 °C/min. The subsequent DSC heating traces were recorded with a rate of 20 °C/min.

Polarized Optical Microscopy (POM). The birefringence and liquid crystalline texture of $P4VP(TDBA)_x$ were examined under a Leica DML POM with a Mettler hot stage (FP-90). The POM samples were made by melting the dried $P4VP(TDBA)_x$ powder sandwiched between a glass slide and a cover glass. After being annealed 5 min at 90 °C, the samples were cooled to room temperature at a rate of 1 °C/min. To observe the isotropization or order−disorder transition, POM heating experiment was also carried out.

X-ray Scattering. A high-flux small-angle X-ray scattering instrument (SAXSess, Anton Paar) equipped with a Kratky block-collimation system and a Philips PW3830 sealed-tube X-ray generator (Cu Kα) was employed to simultaneously measure the small-angle and wide-angle X-ray scattering (WAXS and SAXS) of the dried $P4VP(TDBA)_x$. The one-dimensional (1D) scattering patterns were recorded on an imaging plate with a pixel size of 42.3 × 42.3 μm^2 which extends to the high-angle range (the q range covered by the imaging plate is from 0.06 to 29 nm^{-1}, $q = 4\pi \sin \theta/\lambda$, where λ is the wavelength of 0.1542 nm and 2θ the scattering angle). The scattering angles were calibrated with silver behenate. The original experimental data such as data acquisition, background subtraction, and data reduction were handled by Anton Paar SAXSquant 1.01 software and PCG software package. Before measurement, the $P4VP(TDBA)_x$ samples were further annealed at 100 °C for 2 h followed by cooling to room temperature at a rate of 0.5 °C/min. A temperature control unit (Anton Paar TCS300) in conjunction with the SAXSess was utilized to study the structure evolution as a function of temperature.

RESULTS AND DISCUSSION

Formation of Hydrogen Bonding between P4VP and TDBA. The formation of hydrogen bonds between the carboxylic acid group of TDBA and the pyridine nitrogen of P4VP was investigated by FTIR. Compared with that of pure P4VP, the FTIR results showed that addition of TDBA mainly

dx.doi.org/10.1021/ma301783h | Macromolecules 2012, 45, 8760−8769

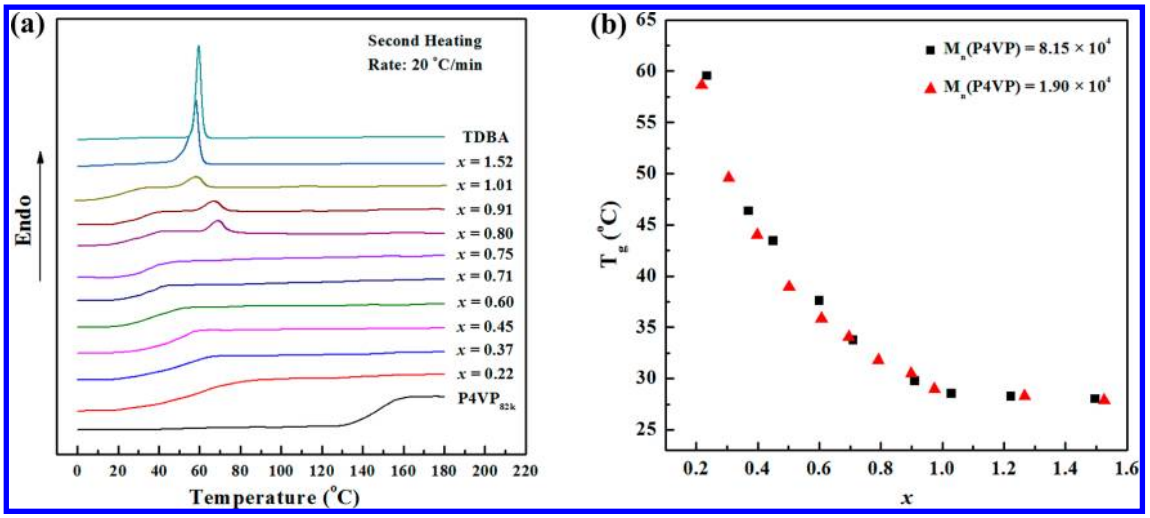

Figure 3. (a) DSC traces of the $P4VP_{82K}(TDBA)_x$ recorded during the second heating at a rate of 20 °C/min. (b) Glass transition temperature (T_g) of $P4VP(TDBA)_x$ at a function of molar ratio x.

affected the bands related to those stretching modes of pyridine ring, which are at 1597, 1415, and 993 cm^{-1}.[40,41] The same as that reported in the literature,[42−44] these bands shift to higher wavenumbers due to the formation of hydrogen bonding. Figure 1a presents the FTIR spectra in the 1300−1650 cm^{-1} of $P4VP_{82K}(TDBA)_x$ with different molar ratio x. For comparison, the spectra of pure P4VP and TDBA are included in the same picture. Apparently, the relative intensities of pyridine bands at 1415 and 1597 cm^{-1} are decreased with increasing x. Meanwhile, a new band at 1604 cm^{-1} becomes more and more obvious, which shall be attributed to the pyridine complexed with the carboxylic acid. Figure 1b shows the variation of the spectra in the 950−1080 cm^{-1} region. The addition of TDBA causes the appearance of a distinct band at 1009 cm^{-1} belonging to neither the pure P4VP nor TDBA, which shall arise from the formation of hydrogen bonding between P4VP and TDBA.[18] The same situation was observed for the samples with $P4VP_{19K}$.

We further estimated the fraction of pyridine groups of P4VP involved in the formation of hydrogen bonding, which may give the "real" complex ratio. Figure 2a describes an enlarged FTIR spectrum of $P4VP_{82K}(TDBA)_{0.35}$ in the region of 1545−1630 cm^{-1}, wherein four bands can be well separated by deconvolution of the rather broad absorption peak.[26] The band at 1597 cm^{-1} is characteristic for the "free" pyridine; the band at 1607 cm^{-1} resulted from the pyridine hydrogen bonded with carboxylic acid. The remaining two bands at 1582 and 1557 cm^{-1} belong to benzene ring of TDBA and pyridine ring, respectively, both insensitive to the hydrogen-bonding interaction. To deconvolute these peaks, the Gaussian amplitude function was used to fit the data, as shown in Figure 2a. The fraction of hydrogen-bonded pyridines ($f_{COOH-pyridine}$) is defined as

$$f_{COOH-pyridine} = \frac{A_{1607}}{A_{1607} + \frac{\alpha_{1597}}{\alpha_{1607}} A_{1597}} \quad (1)$$

where A and α are the peak area and absorption coefficient at 1607 or 1597 cm^{-1}.[45−47] Korhonen et al. studied the mixture of P4VP and a carboxylic acid compound.[48] Using the inert absorption at 1557 cm^{-1} as the reference, they demonstrate that the absorption cross sections of the free and hydrogen-bonded P4VP peaks at 1597 and 1607 cm^{-1} is hardly changed upon complexation, and thus $\alpha_{1597}/\alpha_{1607} \approx 1$. In our case, we also confirmed that the ratio of the peak area of 1557 cm^{-1} band with respect to the total area of all three bands (i.e., $A_{1557} + A_{1597} + A_{1607}$) was remained essentially constant of ~0.12, regardless the variation of composition. Consequently, eq 1 can be reduced to

$$f_{COOH-pyridine} = \frac{A_{1607}}{A_{1607} + A_{1597}} \quad (2)$$

After using the inert absorption at 1557 cm^{-1} to normalize the FTIR spectra, we estimated the value of $f_{COOH-pyridine}$ as a function of the molar ratio x, of which the result is shown in Figure 2b. Apparently, before some point of $x \approx 0.60$, a linear relationship can be observed with a slope of 0.94 for both $P4VP_{82K}$ and $P4VP_{19K}$, meaning that almost all of the TDBA molecules added are grafted to the P4VP chain. It is conceivable that when the number of pyridine groups is significantly exceeded, the balance shifts toward the formation of intermolecular hydrogen bonding and the complexation is nearly complete. However, Figure 2b indicates that further increasing x leads to a deviation from the linear behavior, and finally the value of $f_{COOH-pyridine}$ reaches a plateau at $x > 0.90$. This implies that after more than a half of pyridine groups are incorporated with the rather bulky benzoic acid derivative, the space near the P4VP chains may be quite crowed, and thus the new coming TDBA molecules will feel less opportunity to occupy a proper binding side. Meanwhile, the TDBA molecules themselves have a large tendency to form intermolecular association such as a dimeric structure, which can compete with the hydrogen bonding between the pyridine and carboxylic acid.[49] The intermolecular hydrogen bonding is saturated at $x >$ 0.9. Even with x much larger than the stoichiometry, the value of $f_{COOH-pyridine}$ remains constant. We also observed that at $x >$ ~0.60 the change of $f_{COOH-pyridine}$ is molecular weight dependent. For $P4VP_{82K}(TDBA)_x$ and $P4VP_{19K}(TDBA)_x$, the values of upmost $f_{COOH-pyridine}$ are around 67% and 73%, respectively. This implies that the saturated complexation level is related to the entanglement of P4VP chains. For the longer chains which are more entangled, the initially embedded interaction sites of pyridine might be difficult to migrate to the interface between the domains of P4VP and TDBA. As some

dx.doi.org/10.1021/ma301783h | Macromolecules 2012, 45, 8760−8769

binding sites on the P4VP with larger molecular weight are hidden, the degree of complexation is reduced.

Thermal Behaviors of P4VP(TDBA)$_x$. Thermal behaviors of P4VP(TDBA)$_x$ with different x was examined using DSC. It is well-known that atactic P4VP is typically amorphous with a glass transition temperature (T_g) around 140 °C. TDBA possesses a solid-to-liquid transition at ~59 °C, and no other transition can be observed during cooling and heating. This nonmesogenic benzoic acid molecule is crystalline at low temperature and cannot render liquid crystalline property. When P4VP and TDBA are mixed together, TDBA crystallization and intermolecular hydrogen-bonding interaction undergo competition with each other. We found that the latter one can dominant the phase behavior of P4VP(TDBA)$_x$ at x < 1.00, similar to other polymer−surfactant systems which can form mesophase.[18,24]

Figure 3a depicts DSC traces of P4VP$_{82K}$(TDBA)$_x$ with various x. The addition of TDBA leads to a dramatically reduced T_g in comparison with that of the pristine P4VP. Since TDBA can hydrogen bond with P4VP at a molecular level, it acts effectively as a plasticizer for P4VP.[48−50] Meanwhile, the hydrogen-bonding interaction largely prevents the crystallization. The dependence of T_g for P4VP(TDBA)$_x$ on the molar ratio x is summarized in Figure 3b. After a rapid decrease with increasing x, the value of T_g finally levels off at $x \geq 1.00$. Molecular weight of P4VP has little effect on T_g of the complex, implying that the P4VP$_{19K}$(TDBA)$_x$ and P4VP$_{82K}$(TDBA)$_x$ complexes may share a same phase behavior.

When a large amount of TDBA was added, the thermal behavior of P4VP(TDBA)$_x$ looks a little more complicated. As shown in Figure 3a, in addition to the glass transition, the DSC heating trance of x = 1.01 presents a broad and weak endotherm peak at a temperature slightly lower than that of the pure TDBA at 59 °C, which can be attributed to the melting of the crystallized TDBA. This indicates that after the hydrogen bonding between P4VP and TDBA is saturated, the excessive TDBA molecules are macrophase separated from the complex. For the samples with x > 1, more TDBA can crystallize, giving more clearly the melting peak. Samples with the x value slightly smaller than 1 can also render a small endotherm upon heating. However, for x = 0.80 and 0.91, the temperature of endothermic peak is obviously higher than that of the pure TDBA. Since no evidence of TDBA crystals could be found in WAXS experiments (see below), more likely, the endothermic peak is associated with the order−disorder transition[19] other than the melting of TDBA. One possible reason to account for this endotherm is that some pair of hydrogen bonding got disassociation. However, why the samples with lower x do not exhibit the endothermic process during the order−disorder transition is not known at this moment. The DSC results suggest that for x < 1.00 there should be no macrophase separation, although the FTIR experiment indicates that at x > 0.60 quite a few TDBA molecules do not hydrogen bond to P4VP.

Scattering Behaviors of P4VP(TDBA)$_x$. Hydrogen-bonding interaction between P4VP and TDBA may couple the two components together to form mesomorphic structures. We found that the phase behavior of P4VP(TDBA)$_x$ showed clearly a composition dependence. Figures 4 and 5 depict the X-ray scattering results of P4VP$_{82K}$(TDBA)$_x$ and P4VP$_{19K}$(TDBA)$_x$ recorded at room temperature, respectively, wherein the patterns of pristine PV4P and TDBA are included for comparison. For P4VP, no scattering feature appears in the

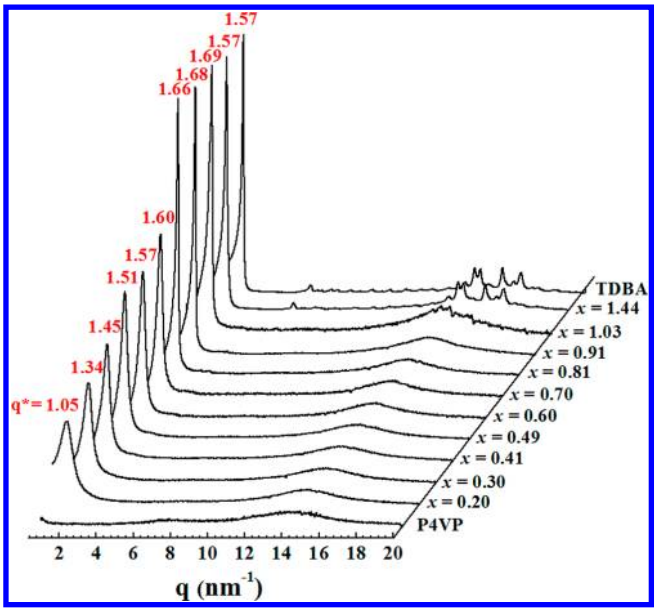

Figure 4. Set of X-ray scattering patterns of P4VP$_{82K}$(TDBA)$_x$ with various x.

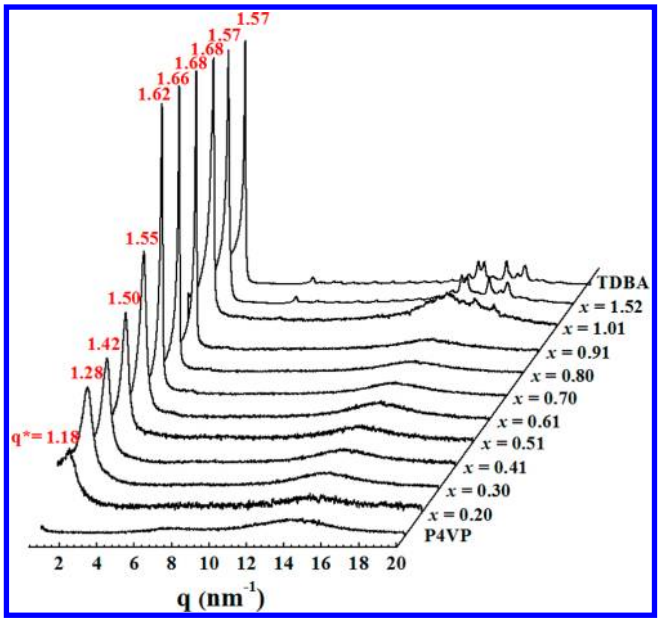

Figure 5. Set of X-ray scattering patterns of P4VP$_{19K}$(TDBA)$_x$ with various x.

low-angle region, while in the high-angle region two amorphous halos with the maxima located at q = 7.4 and 14.1 nm^{-1} can be observed. The scattering experiment demonstrates clearly that the pure TDBA is crystalline. In the low-angle region, the diffractions of TDBA with a q ratio of 1:3 can be observed, of which the first-order peak corresponds to a d-spacing of 4.2 nm. This dimension is nearly twice of the TDBA molecular length of 2.2 nm estimated with an assumption that the alkyl tails adopt an all-trans conformation. Therefore, the TDBA molecules may form a bilayer structure within its crystal, wherein the TDBA might be slightly tilted with respect to the layer normal or the tail ends of TDBA is partially interdigitated.

As shown in Figures 4 and 5, P4VP(TDBA)$_x$ samples with x < 1.00 just display an amorphous scattering in the high-angle region. Therefore, in a wide range of x, TDBA losses the

dx.doi.org/10.1021/ma301783h | Macromolecules 2012, 45, 8760−8769

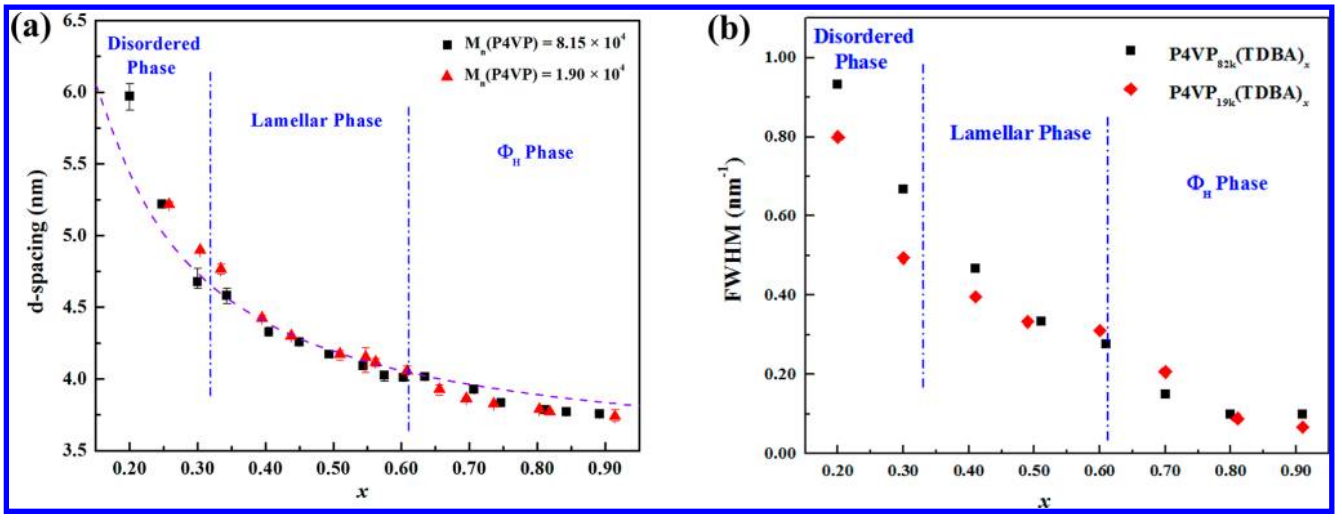

Figure 6. The *d*-spacing (a) and the full width at half-maximum (fwhm) (b) of the low-angle scattering peak as a function of *x* for P4VP(TDBA)$_x$. The dashed line in (a) is a fitting of *d*-spacing ~ 1/*x*, which especially agrees well with data of the lamellar phase.

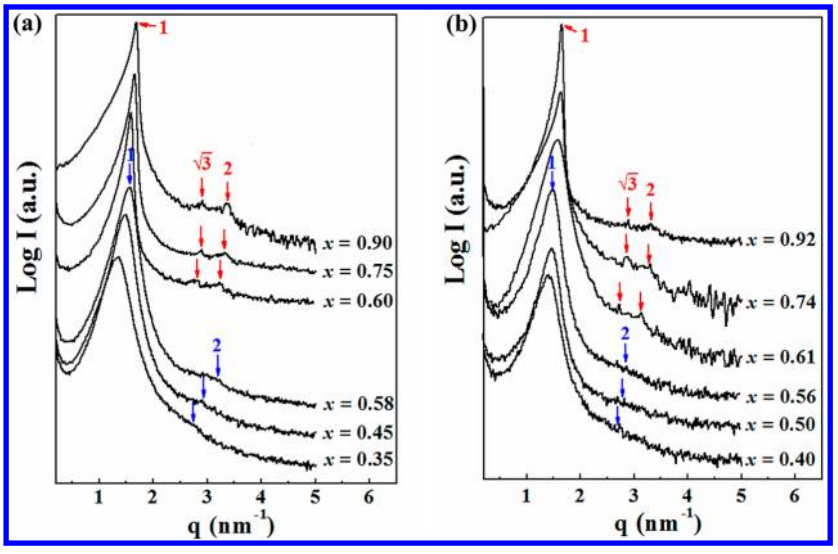

Figure 7. SAXS profiles of P4VP$_{82K}$(TDBA)$_x$ (a) and P4VP$_{19K}$(TDBA)$_x$ (b) with various *x* ranging from 0.30 to 0.90.

crystalline order after it is mixed with P4VP. On the other hand, the samples give a scattering peak in the low-angle region of $q < 3$ nm^{-1}, which certainly arises from the complexation between TDBA and P4VP. We presume that while the intermolecular hydrogen bonding can prevent the crystallization of TDBA, it induces a sort of ordering of the complex on the nanometer scale. At $x \approx 1.00$, tiny diffraction peaks of TDBA crystal are observed; further increasing *x* leads the TDBA crystal diffraction to be dominant. Of particular interesting is that how the mesophase structure develops with varying the molar ratio *x*. The low-angle scattering peak becomes narrow and increases in intensity with increasing *x*. This implies that the more TDBA molecules are added, the better the ordering of the mesophase is formed. Later on we will focus on the phase behaviors of samples without macrophase separation at $x < 1.00$.

Phase Structures of P4VP(TDBA)$_x$. Figure 6a summarizes the *d*-spacing of the low angle scattering peak as a function of *x*, wherein each point represents the average value of the data measured from at least three different samples with a same *x*. In general, the tendency shown in Figure 6a is similar to that reported; namely, increasing *x* leads to the decrease of *d*-spacing.[38] In this case, one may assume that the system of P4VP(TDBA)$_x$ forms a lamellar structure with the sublayer of P4VP chains squeezed by two adjacent sublayers of TDBA. According to ten Brink and Ikkala, such a layer structure possesses its long period *L* linearly proportional to the reciprocal of *x*. The dashed line in Figure 6 is the fit based on 1/*x* behavior. In general, the fitted line represents the experimental data quite well. However, careful examination can reveal that the *d*-spacings of $x < 0.30$ are all above the line. On the other hand, the data of $x > 0.60$ systematically locate underneath the line, although they are very close to each other. These small deviations indicate that the P4VP(TDBA)$_x$ complex may form not only a lamellar phase but also other phases when the molar ratio *x* is changed. Figure 6b presents the full width at half-maximum (fwhm) of the low-angle scattering peak varying with the molar ratio *x*. The value of fwhm decreases drastically at $x < \sim 0.3$ and goes to level off afterward. Furthermore, at $x \sim 0.6$, the second drop of fwhm can be observed. It is interesting to note that Figures 6a,b

dx.doi.org/10.1021/ma301783h | *Macromolecules* 2012, 45, 8760−8769

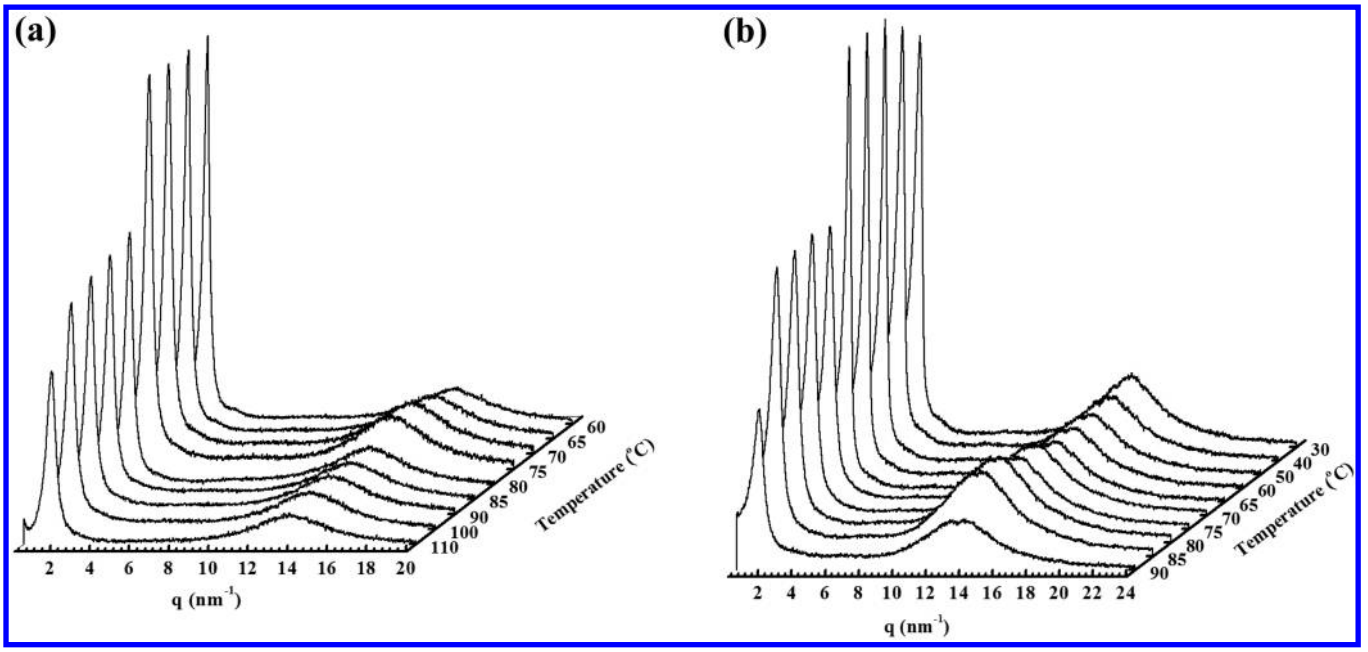

Figure 8. Sets of SAXS profiles of $P4VP_{82K}(TDBA)_x$ recorded at different temperatures during heating: (a) $x = 0.58$; (b) $x = 0.81$.

exhibit rather similar molar ratio dependence, which can be related to the phase behavior of $P4VP(TDBA)_x$.

To identify the phase structure of $P4VP(TDBA)_x$, we also examined the samples under POM. For $x < \sim 0.30$, no birefringence was detected. Note that the samples with $x < \sim 0.30$ in fact only give a broad scattering peak in the low-angle region. Therefore, we consider that the small amount of TDBA added just induces a density fluctuation within the mixture, and no mesophase such as lamella can be really formed. After more TDBA molecules were grafted to the P4VP chain via hydrogen bonding, liquid crystal textures could be observed at $x > \sim 0.30$ (see the Supporting Information). It is very interesting to note that our SAXS results of samples with $x > \sim 0.30$ can render the second-order scattering, which becomes stronger and more obvious with increasing x (Figure 7). Although the second-order scattering is always diffusive, implying that the long-range order of mesophase is not well developed, it can certainly confirm the formation of ordered structure and, moreover, can reflect what the mesophase structures the $P4VP(TDBA)_x$ samples form.

As shown in Figure 7a, the samples of $P4VP_{82K}(TDBA)_x$ with $x < 0.60$ possess the two low-angle scattering with a q-ratio of 1:2, a manifestation of the lamellar phase. Interestingly, for the samples with $x > 0.60$, the scattering peaks up to the third order can be detected. For example, the three peaks of $P4VP_{82K}(TDBA)_{0.90}$ locate at $q = 1.69$, 2.92, and 3.38 nm^{-1} with the q-ratio of $1:\sqrt{3}:2$, featuring a hexagonal lattice with the lattice parameter a of 4.30 nm. Since the amorphous high angle scattering indicates no positional order on the subnanometer scale, we consider that the sample forms a Φ_H phase. Note that the sample with $x = 0.58$ renders a rather broad second-order scattering with the peak maximum located at $2q_1$ (q_1 is the position of the first-order scattering), while the sample with $x = 0.60$ shows the second-order scattering at $\sqrt{3}q_1$. This possibly means that $x \sim 0.60$ is a transition boundary between lamellar and Φ_H (or cylinder) phases. Figure 7b shows that the $P4VP_{19K}(TDBA)_x$ complex also exhibits the behavior similar to that of $P4VP_{82K}(TDBA)_x$. In this case, combining the X-ray scattering and POM results, we can distinguish three regimes of the $P4VP(TDBA)_x$ in terms of the molar ratio x: for $x < 0.30$, the sample is disordered with local density fluctuation; for $0.30 < x < 0.60$, a lamellar phase exists; for $x > 0.60$, the sample forms a Φ_H phase.

Upon heating experiments, we could detect the isotropization or order−disorder transition of $P4VP(TDBA)_x$. The thermal SAXS results of $P4VP_{82K}(TDBA)_{0.58}$ and $P4VP_{82K}(TDBA)_{0.81}$ are shown in Figures 8a and 8b, respectively. When being heated up to ~75 °C, the scattering peak of $P4VP_{80K}(TDBA)_{0.58}$ which can form lamellar phase becomes broader and its intensity drops abruptly, indicating the order−disorder transition.[19] Such a transition of $P4VP_{82K}(TDBA)_{0.81}$ happens at ~65 °C, in good accordance with the location of endothermic peak shown on the DSC heating trace. The samples lost the birefringence completely under POM after the order−disorder transition, indicating that the sample entered in the isotropic state. Our POM heating experiments of $P4VP(TDBA)_x$ confirmed that the order−disorder transition temperature of lamellar phase was nearly 10 °C higher than that of the Φ_H phase.

Microphase Separation in the Mesophases of P4VP-(TDBA)$_x$. To understand the molecular packing in the mesomorphic structures of $P4VP(TDBA)_x$, we should consider the segregation of different components with different chemical properties within the system. We assume that the microphase-separated structures contains regular and shape interface, although in reality the case must be much complicated particularly when the molar ratio x is small. However, this simplest approximation can let us catch the basic feature of the molecular arrangement in the mesophase.

For the lamellar phase of polymer−surfactant systems, the linear relationship of $L \propto 1/x$ has been explained by ten Brinke and Ikkala et al.[38] using a simple scaling argument. The assumption taken by them is that the surfactant layer thickness is invariant with varying the composition of the complex, which should be reasonable. In this case, the intercept of L vs $1/x$ plot is the surfactant layer thickness (L_S). As shown in Figure 9, the value of L_S is obtained to be 3.2 nm, which is much larger than the extended length of 2.2 nm of TDBA. Therefore, most likely,

dx.doi.org/10.1021/ma301783h | Macromolecules 2012, 45, 8760−8769

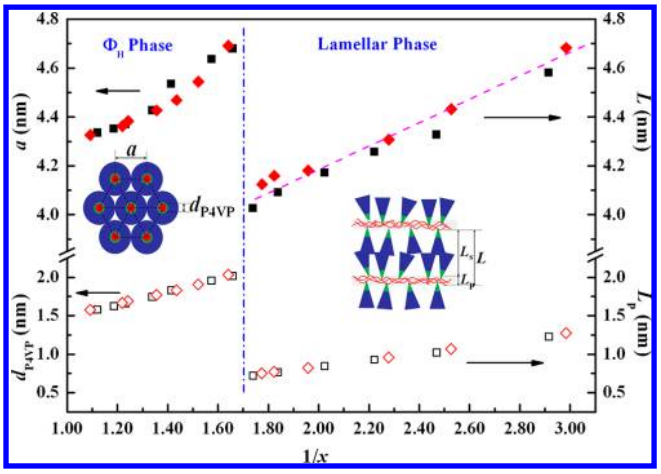

Figure 9. Dimensions (solid symbols) of lamellar and Φ_H phase as functions of $1/x$. The sizes of P4VP domains (open symbols) in the mesophases are also plotted. d_{P4VP} denotes the diameter of P4VP core in the Φ_H phase, and L_P represents the thickness of P4VP sublayer in the lamellar phase. Black and red symbols correspond to $P4VP_{82K}(TDBA)_x$ and $P4VP_{19K}(TDBA)_x$, respectively. The dashed pink line is the linear fit of the long period L of lamellar phase, of which the intercept of 3.2 nm gives the surfactant layer thickness L_S. The d_{P4VP} of Φ_H phase was estimated based on eq 3b.

the $P4VP(TDBA)_x$ lamella contains two 1.6 nm thick sublayers of TDBA, implying that the alkyl tails of the small molecules are coiled rather than extended. Keeping the L_S as a constant, we may estimate the thickness of the P4VP (L_P) for the lamellar phase, of which the results fairly agrees with that of P4VP sublayer in the P4VP–pentadecylphenol complex and PVI–aliphatic acid complex with $x = 1.00$.[25,49] For $P4VP(TDBA)_x$, the value of L_P is reduced from 1.4 to 0.8 nm when x changes from 0.30 to 0.60 (see Figure 9). This means that when more TDBA molecules successfully bond to P4VP, the conformation of P4VP becomes more oblate, and thus the chain is subjected to a stronger confinement imposed by the TDBA sublayers.

Figure 9 also shows the lattice parameter a of the Φ_H phase as a function of $1/x$, which is no longer follows the linear behavior. In the Φ_H phase, the building block is the column with microphase separation along the radial direction. The P4VP chains should be confined in the center of the column, surrounded by the continuous phase of TDBA molecules. The detailed molecular packing behavior will be discussed in the next subsection.

Lamella-to-Cylinder Transition of $P4VP(TDBA)_x$. It is very interesting to realize that $P4VP(TDBA)_x$ can develop into Φ_H phase at $x > \sim 0.60$. Once the P4VP sublayer thickness reaches 0.8 nm at x of ~0.60, further compressing the chain conformation to be more planar in the lamellar structure becomes physically unreasonable. In order to incorporate with more TDBA molecules, the mesophase of $P4VP(TDBA)_x$ can change its more or less flat interface to a curved one, resulting in a cylinder phase. As shown in Figure 2b, the increase of $f_{COOH-pyridine}$ deviates from the linear behavior after x exceeds ~0.60. This turn point is in accordance with that of the phase transition observed. The increment of $f_{COOH-pyridine}$ slows down with further increasing x, indicating that the formation of hydrogen-bonding interaction becomes more difficult when P4VP is confined inside the column of Φ_H phase. However, the hydrogen-bonding interaction still provides the driving force for the Φ_H formation.

In polymer–surfactant systems, cylindrically closed packing morphology can be observed when the highly ionic polymer chain and surfactant molecules can complex together via the strong electrostatic interaction.[36,37] To the best of our knowledge, $P4VP(TDBA)_x$ is the first example to exhibit Φ_H phase based on intermolecular hydrogen-bonding interaction. We consider that the structure of TDBA with three dodecyl tails plays an important role. The large nonpolar portion of TDBA certainly enhances the microphase separation.[18] Moreover, similar to the cases that reported by Beginn et al.[36] and Tong et al.,[37,51] the shape of TDBA which is more or less fan-like facilitates the formation of Φ_H phase. In the microphase-separated structure, the bulky TDBA molecule requires more interfacial area in comparison with the linear surfactant molecule. When more and more TDBA molecules form hydrogen bonding with P4VP, the nearly flat interface of lamellar structure becomes unfavorable eventually, and consequently, a lamella-to-cylinder transition occurs.

According to ten Brinke and Ikkala et al., after complexation of polymer and surfactant, the system can be simply separated into two parts of polar and nonpolar, of which the latter one consists of pure alkyl groups. For $P4VP(TDBA)_x$ studied here, the molar masses of the P4VP repeating unit, the TDBA molecule, and the three dodecyl tails are 105, 674, and 507 g/mol, respectively. Assuming the densities of the highly polar part and the pure alkyl part to be ~1.2 and ~0.9 g/cm^3,[3,24] respectively, the volume fraction of alkyls (f_{tail}) in $P4VP(TDBA)_x$ can be estimate as $f_{tail} = (507x/0.9)/[507x/0.9 + (167x + 105)/1.2]$. Accordingly, the volume fraction of P4VP (f_{P4VP}) can be written as $f_{P4VP} = (105/1.2)/[507x/0.9 + (167x + 105)/1.2]$. These two relationships can be reduced to

$$f_{tail} = 563x/(702x + 88) \quad (3a)$$

$$f_{P4VP} = 88/(702x + 88) \quad (3b)$$

For the lamellar phases at $x = 0.30$ and 0.60, the values of f_{P4VP} are ~0.29 and 0.20, respectively, corresponding to the P4VP sublayer thicknesses of ~1.4 and 0.7 nm, in good agreement with the data shown in Figure 9. The coincidence indicates that eq 3 can be applied to make a rather reasonable estimation of the volume fraction. We find that at $x = 0.60$ the value of f_{tail} of $P4VP(TDBA)_x$ is of ~0.66. Interestingly, this value is very close to the theoretically predicated boundary between the lamellar and cylinder phase which locates at $f_{tail} = 0.68$.[24] Further increasing x will certainly lead the complex to enter the cylinder phase, as evidenced by our SAXS result. In this case, the lamella-to-cylinder transition of $P4VP(TDBA)_x$ can also be understood based on the volumetric consideration.

The lamella-to-cylinder transition should associate with the conformation changing of P4VP chain from oblate coil to more extended one. At $x = 0.30$, the value of f_{tail} is of 0.56, which is well away from the theoretical boundary of lamellar phase. However, we find that the complex with $x < 0.30$ does not form well-ordered lamellar structure and just exhibits a density fluctuation. This may be due to that the low grafting density cannot induce strong enough microphase separation[18] so that the P4VP chains would adopt a three-dimensional coil rather than an oblate conformation. Once the microphase separation makes the P4VP chain more oblate, the interface between the sublayers of P4VP and TDBA becomes shaper, resulting in the lamellar phase which can detected by X-ray scattering. For the Φ_H phase of $P4VP(TDBA)_x$, the lattice parameter a of 4.6 nm at $x \approx 0.60$ is almost identical to the layer thickness in the

dx.doi.org/10.1021/ma301783h | Macromolecules 2012, 45, 8760–8769

vicinity of x of 0.30 where the complex just forms clearly a lamellar phase (see Figure 9). According to eq 3b, f_{P4VP} is of ~0.17 at $x \approx 0.60$. Therefore, the diameter of the cylindrical core of P4VP (d_{P4VP}) embedded in the matrix of TDBA should be of ~2.0 nm, significantly larger than the P4VP sublayer thickness of ~0.8 nm at the x slightly smaller than 0.6. This means that confinement on P4VP chains is partially released after the lamella-to-cylinder transition, and thus the chains can gain more conformational entropy which is thermodynamically favorable. Meanwhile, the TDBA size becomes around 1.3 nm [i.e., $(4.6 - 2.0)/2$], implying that the alkyl tails are more coiled. At $x \approx 0.90$, the P4VP core diameter d_{P4VP} can be estimated to be ~1.6 nm, and the TDBA molecules remain a constant size of ~1.3 nm. It is conceivable that when more TDBA molecules are added, the P4VP chain needs to expose more of its complementary binding sites of pyridine on the interface. This will cause the P4VP chain to be more extended, which should be responsible for the reduction of the hexagonal lattice with increasing x. Continuously shrinking the cylinder may finally leads to the P4VP chain with an overall rod-like conformation. However, in that case, the system will face an unaffordable penalty of entropy. When the hydrogen-bonding interaction saturates, the a dimension and also the P4VP core diameter will be no longer changed. With the Φ_H phase, the P4VP(TDBA) complex may be analogous to dendronized polymers.[52−54] However, at this moment, we do not know that the P4VP core within the Φ_H phase consists of one chain or a few chains.[35,55−57]

CONCLUSIONS

In summary, the phase behavior of P4VP(TDBA)$_x$ complex with different molar ratio x of TDBA to P4VP repeating unit has been investigated. As a derivative of benzoic acid, TDBA contains three alkyl tails with the shape more or less fan-like. The intermolecular hydrogen-bonding interaction between TDBA and P4VP is confirmed by FTIR experiment. Quantitative analysis of the FTIR results reveals that at $x <$ ~0.60 almost all of the added TDBA molecules are hydrogen bonded to the P4VP chains. The hydrogen bonding becomes incomplete when x exceeds 0.60 and saturates at $x > 0.90$. For the complex with $x \geq 1.00$, macrophase separation occurs, wherein the excessive TDBA crystallizes. Upon using various techniques, we have found that addition of small amount of TDBA (i.e., $x <$ ~0.30) just causes a density fluctuation. At $x >$ ~0.30, P4VP(TDBA)$_x$ complex can form a mesomorphic structure. The lamellar phase is observed within the range of ~0.30 $< x <$ ~0.60, of which the long period L is linearly proportional to $1/x$. Interestingly, a cylinder or hexagonal columnar (Φ_H) phase can be identified at $x >$ ~0.60. The lamella-to-cylinder transition can be understood based on a volumetric argument. Considering the phase separation between the nonpolar part of alkyl tails and the polar part, the volume fraction f_{tail} of the tails at $x = 0.60$ is estimated to be 0.66, rather close to the theoretical boundary of lamella−cylinder phase transition located at f_{tail} of 0.68. We consider that the large nonpolar part of TDBA enhances the microphase separation of P4VP(TDBA)$_x$, and moreover, the fan-like shape of TDBA facilitates the formation of Φ_H phase. We also roughly estimated the domain size of the P4VP chains in the microphase-separated mesophase using the volumetric analysis. The result suggests that during the lamella-to-cylinder transition the confinement imposed on the P4VP chains by the TDBA molecules may be partially released, which favors the Φ_H formation. The phase structure of P4VP(TDBA)$_x$ changing from lamella to Φ_H phase should be correlated to the change of P4VP conformation from oblate coil to extended one. Therefore, our results can provide some quantitative data for the theoretical analysis of chain conformation transformation. As the hydrogen-bonded polymer−ligand complexes with Φ_H phase possess two-dimensionally positional order and one-dimensional connectivity, they may also be employed as nanostructured functional materials in nanotechnologies.

ASSOCIATED CONTENT

Supporting Information

Polarized optical microscopy (POM) results of P4VP(TDBA)$_x$ complexes. This material is available free of charge via the Internet at http://pubs.acs.org.

AUTHOR INFORMATION

Corresponding Author

*E-mail: eqchen@pku.edu.cn (E.-Q.C.); shuangyang@pku.edu.cn (S.Y.).

Notes

The authors declare no competing financial interest.

ACKNOWLEDGMENTS

This work was supported by the National Natural Science Foundation of China (20990232, 21074003, and 21104001) and the Major State Basic Research Development Program (2011CB606004) from the Ministry of Science and Technology. We are grateful to Prof. An-Chang Shi for discussions.

REFERENCES

(1) Kato, T.; Frechet, J. M. J. *Macromolecules* **1989**, *22*, 3818−3819.
(2) Cao, Y.; Smith, P. *Polymer* **1993**, *34*, 3139−3143.
(3) Ruokolainen, J.; Makinen, R.; Torkkeli, M.; Makela, T.; Serimaa, R.; Ten Brinke, G.; Ikkala, O. *Science* **1998**, *280*, 557−560.
(4) Kato, T.; Mizoshita, N.; Kishimoto, K. *Angew. Chem., Int. Ed.* **2006**, *45*, 38−68.
(5) Pollino, J. M.; Weck, M. *Chem. Soc. Rev.* **2005**, *34*, 193−207.
(6) Hammond, M. R.; Mezzenga, R. *Soft Matter* **2008**, *4*, 952−961.
(7) Ober, C. K.; Wegner, G. *Adv. Mater.* **1997**, *9*, 17−31.
(8) Faul, C. F. J.; Antonietti, M. *Adv. Mater.* **2003**, *15*, 673−683.
(9) Cheng, Y.; Chen, W.; Zheng, C.; Qu, W.; Wu, H.; Shen, Z.; Liang, D.; Fan, X.; Zhu, M.; Zhou, Q. *Macromolecules* **2011**, *44*, 3973−3980.
(10) Yildiz, Ü. H.; Koynov, K.; Gröhn, F. *Macromol. Chem. Phys.* **2009**, *210*, 1678−1690.
(11) Zhang, Q. A.; Bazuin, C. G. *Macromol. Chem. Phys.* **2010**, *211*, 1071−1082.
(12) Bouteiller, L. *Adv. Polym. Sci.* **2007**, *207*, 79−112.
(13) Ten Brinke, G.; Ruokolainen, J.; Ikkala, O. *Adv. Polym. Sci.* **2007**, *207*, 113−177.
(14) Sun, H.; Lee, C.; Lai, C.; Chen, H.; Tung, S.; Chen, W. *Soft Matter* **2011**, *7*, 4198−4206.
(15) de Wit, J.; van Ekenstein, G. A.; Polushkin, E.; Kvashnina, K.; Bras, W.; Ikkala, O.; Ten Brinke, G. *Macromolecules* **2008**, *41*, 4200−4204.
(16) Schubert, U. S.; Eschbaumer, C. *Angew. Chem., Int. Ed.* **2002**, *41*, 2892−2926.
(17) Welterlich, I.; Tieke, B. *Macromolecules* **2011**, *44*, 4194−4203.
(18) Ruokolainen, J.; Torkkeli, M.; Serimaa, R.; Vahvaselkä, S.; Saariaho, M.; Ten Brinke, G.; Ikkala, O. *Macromolecules* **1996**, *29*, 6621−6628.
(19) Ruokolainen, J.; Torkkeli, M.; Serimaa, R.; Komanschek, B. E.; Ikkala, O.; Ten Brinke, G. *Phys. Rev. E* **1996**, *54*, 6646−6649.

(20) Antonietti, M.; Conrad, J.; Thunemann, A. *Macromolecules* **1994**, *27*, 6007−6011.
(21) Ikkala, O.; Ruokolainen, J.; Ten Brinke, G.; Torkkeli, M.; Serimaa, R. *Macromolecules* **1995**, *28*, 7088−7094.
(22) Antonietti, M.; Göltner, C. *Angew. Chem., Int. Ed.* **1997**, *36*, 910−928.
(23) Macknight, W. J.; Ponomarenko, E. A.; Tirrell, D. A. *Acc. Chem. Res.* **1998**, *31*, 781−788.
(24) Ruokolainen, J.; Ten Brinke, G.; Ikkala, O.; Torkkeli, M.; Serimaa, R. *Macromolecules* **1996**, *29*, 3409−3415.
(25) Jiao, H.; Goh, S. H.; Valiyaveettil, S. *Langmuir* **2002**, *18*, 1368−1373.
(26) Gopinadhan, M.; Beach, E. S.; Anastas, P. T.; Osuji, C. O. *Macromolecules* **2010**, *43*, 6646−6654.
(27) Kawakami, T.; Kato, T. *Macromolecules* **1998**, *31*, 4475−4479.
(28) Kato, T.; Kihara, H.; Ujiie, S.; Uryu, T.; Frechet, J. *Macromolecules* **1996**, *29*, 8734−8739.
(29) Rancatore, B. J.; Mauldin, C. E.; Tung, S. H.; Wang, C.; Hexemer, A.; Strzalka, J.; Frechet, J.; Xu, T. *ACS Nano* **2010**, *4*, 2721−2729.
(30) Osuji, C. O.; Chao, C.; Ober, C. K.; Thomas, E. L. *Macromolecules* **2006**, *39*, 3114−3117.
(31) Ruokolainen, J.; Tanner, J.; Ikkala, O.; Ten Brinke, G.; Thomas, E. L. *Macromolecules* **1998**, *31*, 3532−3536.
(32) Fredrickson, G. H. *Macromolecules* **1993**, *26*, 2825−2831.
(33) Chen, X. F.; Shen, Z. H.; Wan, X. H.; Fan, X. H.; Chen, E. Q.; Ma, Y. G.; Zhou, Q. F. *Chem. Soc. Rev.* **2010**, *39*, 3072−3101.
(34) Rosen, B. M.; Wilson, C. J.; Wilson, D. A.; Peterca, M.; Imam, M. R.; Percec, V. *Chem. Rev.* **2009**, *109*, 6275−6540.
(35) Antonietti, M.; Conrad, J. *Angew. Chem., Int. Ed.* **1994**, *33*, 1869−1870.
(36) Zhu, X.; Beginn, U.; Möller, M.; Gearba, R. I.; Anokhin, D. V.; Ivanov, D. A. *J. Am. Chem. Soc.* **2006**, *128*, 16928−16937.
(37) Cheng, Z.; Ren, B.; Shan, H.; Liu, X.; Tong, Z. *Macromolecules* **2008**, *41*, 2656−2662.
(38) Ten Brinke, G.; Ruokolainen, J.; Ikkala, O. *Europhys. Lett.* **1996**, *35*, 91−95.
(39) Percec, V.; Cho, W. D.; Ungar, G. *J. Am. Chem. Soc.* **2000**, *122*, 10273−10281.
(40) Ikkala, O.; Ruokolainen, J.; Ten Brinke, G.; Torkkeli, M.; Serimaa, R. *Macromolecules* **1995**, *28*, 7088−7094.
(41) Ruokolainen, J.; Tanner, J.; Ten Brinke, G.; Ikkala, O.; Torkkeli, M.; Serimaa, R. *Macromolecules* **1995**, *28*, 7779−7784.
(42) Cesteros, L. C.; Isasi, J. R.; Katime, I. *Macromolecules* **1993**, *26*, 7256−7262.
(43) Cesteros, L. C.; Meaurio, E.; Katime, I. *Macromolecules* **1993**, *26*, 2323−2330.
(44) Cesteros, L. C.; Velada, J. L.; Katime, I. *Polymer* **1995**, *36*, 3183−3189.
(45) Gordon, S. H.; Cao, X.; Mohamed, A.; Willett, J. L. *J. Appl. Polym. Sci.* **2005**, *97*, 813−821.
(46) Lee, J. Y.; Painter, P. C.; Coleman, M. M. *Macromolecules* **1988**, *21*, 954−960.
(47) Lichkus, A. M.; Painter, P. C.; Coleman, M. M. *Macromolecules* **1988**, *21*, 2636−2641.
(48) Korhonen, J. T.; Verho, T.; Rannou, P.; Ikkala, O. *Macromolecules* **2010**, *43*, 1507−1514.
(49) Luyten, M. C.; Alberda Van Ekenstein, G. O. R.; Ten Brinke, G.; Ruokolainen, J.; Ikkala, O.; Torkkeli, M.; Serimaa, R. *Macromolecules* **1999**, *32*, 4404−4410.
(50) Valkama, S.; Ruotsalainen, T.; Nykanen, A.; Laiho, A.; Kosonen, H.; Ten Brinke, G.; Ikkala, O.; Ruokolainen, J. *Macromolecules* **2006**, *39*, 9327−9336.
(51) Cheng, Z.; Ren, B.; Zhao, D.; Liu, X.; Tong, Z. *Macromolecules* **2009**, *42*, 2762−2766.
(52) Zhang, A. F.; Shu, L. J.; Bo, Z. S.; Schluter, A. D. *Macromol. Chem. Phys.* **2003**, *204*, 328−339.
(53) Zhang, B. Z.; Wepf, R.; Fischer, K.; Schmidt, M.; Besse, S.; Lindner, P.; King, B. T.; Sigel, R.; Schurtenberger, P.; Talmon, Y.; Ding, Y.; Kroger, M.; Halperin, A.; Schluter, A. D. *Angew. Chem., Int. Ed.* **2011**, *50*, 737−740.
(54) Frauenrath, H. *Prog. Polym. Sci.* **2005**, *30*, 325−384.
(55) Kwon, Y. K.; Chvalun, S.; Schneider, A.; Blackwell, J.; Percec, V.; Heck, J. A. *Macromolecules* **1994**, *27*, 6129−6132.
(56) Rudick, J. G.; Percec, V. *Acc. Chem. Res.* **2008**, *41*, 1641−1652.
(57) Zheng, J. F.; Liu, X.; Chen, X. F.; Ren, X. K.; Yang, S.; Chen, E. Q. *ACS Macro Lett.* **2012**, *1*, 641−645.